On Potential Spectroscopic Detection of Microfossils on Mars

Giuseppe A. Marzo · Romolo Politi · Armando Blanco · Rosario Brunetto · Sergio Fonti · Vincenzo Orofino

Abstract There is much evidence about the ancient presence of water on Mars and it is reasonable to suppose that simple forms of life may have developed during the geological evolution of the planet. In such a case traces of this extinct life could still be present on the planet in form of microfossils included into some geological layer. The rover payloads planned for the next decades will include spectrometers in order to accomplish various scientific tasks. In this respect, we have developed a quantitative model for microfossil inclusions into a crystalline matrix. Such a method foresees some visible effects on measurements obtained via spectroscopic techniques such as infrared reflectance and Raman spectroscopy. In this work we present the quantitative model of the fossilization process and the effects that the microfossil inclusions should have in the real spectra, evaluated by means of computer simulations. Preliminary measurements, in order to provide examples of future model testing, have been performed on samples of homogeneous composition, but with detectable microfossils content, collected at the K–T sequence placed near Gubbio (Italy). The preliminary results are presented and discussed in order to investigate the potential application of such spectroscopic techniques for the detection of extinct life.

Keywords Fossil · Infrared reflectance · Life detection · Mars · Raman spectroscopy

1 Introduction

The ancient Martian climate was probably very different from the current one. Now, Mars is a cold desert with an annually averaged surface temperature close to 210 K and an average atmospheric pressure of about 6 mbar. However, climatic models (Pollack et al.

G. A. Marzo · R. Politi · A. Blanco · R. Brunetto · S. Fonti · V. Orofino
Physics Department, University of Salento, C.P. 193, Lecce 73100, Italy

G. A. Marzo (✉)
Astrophysics Laboratory, via Arnesano C.P. 193, Lecce 73100, Italy
e-mail: giuseppe.marzo@le.infn.it

1987; Forget and Pierrehumbert 1997; Yung et al. 1997) suggest the possibility that, in the past, the surface temperature and the atmospheric pressure were high enough to allow a stable presence of liquid water on the surface (Malin and Carr 1999; Hynek and Phillips 2003; Howard et al. 2005; Bibring et al. 2006). In particular, early Mars may have experienced episodes of warmer and wetter climate with a thicker atmosphere, providing the necessary greenhouse effect, and a higher geothermal heat flux (Pollack et al. 1987; Fanale et al. 1992; Squyres and Kasting 1994). Expected products of such a history would be extensive carbonate and sulfate rock layers in crater lake sediments. In this scenario, conditions on Mars may even have been Earth-like with the consequent development of simple forms of life. If this was the case, the possible presence of microorganism fossil marks could be detectable (Banfield et al. 2001). In addition, the growing interest related to the evolution of the Martian environment has stimulated the scientific community to develop a number of experiments in order to explore the planet by means of both space-crafts and rover missions. The possibility of examining at close range selected areas of the planet, searching for mineralogic components and morphological features, opens the chance of detecting some marks of extinct life such as microfossil inclusions.

The detection of a fossil mark is not a straightforward process, in particular referred to microorganism fossils (hereinafter *microfossils*). The simple morphology of microfossils can be mimicked by non-biological mineral microstructures, therefore discriminating between true microbial fossils and microscopic pseudofossil can be difficult (Schopf and Walter 1983; Mendelson and Schopf 1992). Usual techniques involve the analysis of the inclusion morphology, and some chemical and physical analysis such as the measurement of residual traces of constituent-of-life elements. However, spectroscopic techniques are easy to implement on mission payloads and are usually present on rovers in order to accomplish various scientific tasks. In this work we investigate the possibility of exploiting an appropriate combination of such spectroscopic techniques to check for the presence of microfossil traces and, if possible, to individuate some candidate features of extinct life.

First the presence of microfossil inclusions, together with a probable fossilization process for the Martian environmental conditions, is greatly simplified in order to be quantitatively modeled. The results of the modeling process are then presented, evidencing some spectroscopic effects appearing in sample spectra relative to samples with micro-fossil inclusions. Finally, some preliminary measurements are provided as examples of the measurement campaign, which can be performed in order to assess and quantify the detectability of the predicted effects.

2 A Model for Microfossil Inclusions

Fossilization is not a random process but the direct consequence of well defined conditions taking place in the environment around an organism after its death. The main process is the burial of the body, otherwise the remnant is destroyed by bacteria and oxidization pro-cesses. In order to obtain a fossil, it is necessary that some substance permeates through the sediment and changes the physical and chemical equilibrium of the organic decomposition. One of the most common material providing such a preservation is the calcium carbonate by means of many different fossilization processes. In the case of a fossil obtained from a microorganism included into an evaporitic sediment, such as calcite, the involved process is mineral replacement (Westall 1999). In such a process, the majority of the original molecular constituents of the microorganism are replaced by others carried by the water flowing through the sediments, leaving, in some cases, only traces of organic matter

(Schopf et al. 2002). When the replacement process occurs slowly, the microorganism keeps its original structure (Westall 1999). The reasonable consequence of the described process is a different crystallization velocity between the volume occupied by the microorganism and the rest of the matrix. In case of replacement, the crystallization of the matrix occurs at the same time in each point; therefore, it can be considered basically uniform over large volumes (compared to the microorganism scale). On the other hand, the organism structure experiences the replacement of the pristine materials with those of the matrix and, then, the subsequent crystallization. Obviously, this mechanism implies that the crystallization takes place at a different time with respect to the matrix, but also at different times between different areas of the organism, in particular considering areas with different depth in the organic structure. The combined effect of the time-dependent crystallization and the spatial inhomogeneity, introduced by the organic structure, is that a homogeneous growth of the crystalline lattice of the matrix is not possible.

The calcite lattice is formed by the iteration over a three-dimensional scale of a single calcite cell. The chemical formula of calcite is $CaCO_3$ arranged in such a structure that implies the presence of one optical axis only (Sass et al. 1957). The basic assumption of the model is that only calcite is present into the sedimentary deposit. In such a case, when the evaporation occurs, the forming calcite cells tend to coalign forming ideal mono-crystals. Such monocrystals are composed of many unit cells and, in absence of spatial or physical inhomogeneities, are generally disposed along a preferential plane that is the plane of the forming layer. During the sedimentary layer formation, the buried microorganism is not exposed to the organic decomposition process and can be regarded as a complex spatial inhomogeneity hardly influencing the monocrystals sedimentation. Inside the volume of the microorganism inclusion, the crystallization takes place at different time for different areas. Each area can be formed by many calcite cells and can be represented as a microdomain with a random orientation with respect to the cells axis. The resultant microscopical effect is a patchwork of crystalline microdomains, disposed with a total angular randomness, replacing the microorganism volume and reproducing its morphology.

We are aware that such level of approximation is quite inadequate to fully characterize a microfossil; since it is based on ideal, therefore unrealistic, physical conditions and skips the chemistry of the fossilization process. However, in spite of such a simplicity, this approach provides a useful scheme, which allows to quantitatively describe the spectroscopic effects of microfossil inclusions into a sample with the typical sensitivity of the examined techniques. In the next sections the described model is used as the starting base, in order to study how the amount of microfossil inclusions can influence infrared and Raman spectra of pure calcite.

2.1 Infrared Spectroscopy

Unless it is coupled with a microscope, a reflectance spectrometer has a field of view much larger than the dimension of a fossil inclusion, which is typically of some tens microns. Therefore the case of a sample of calcite with microfossil inclusions, as seen by such a spectrometer, can be regarded as the case of a sample of a pure calcite matrix with inclusions of pressed calcite powder that simulate the disarrangement due to the microfossils presence, since each grain is regarded as a crystalline microdomain. Such a sample has a reflectance spectrum that is given by the contribution of the ordinary and extraordinary components of the radiation field, depending on the observation angle, and the

spectrum due to the pressed calcite powder. In the hypothesis of radiation propagating from vacuum to calcite, the synthetic reflectance spectrum R is the sum of each contribution:

$$R = Area_{ord}R_{ord} + Area_{ext}R_{ext} + Area_{pow}R_{pow} \tag{1}$$

The coefficients $Area_{ord}$, $Area_{ext}$ and $Area_{pow}$ are related to the real abundance in ordinary mode, extraordinary mode and pressed powder respectively, while R_{ord}, R_{ext} and R_{pow} are the reflectance of each mode given by Hapke (1993):

$$R_j = \frac{(n_j - 1)^2 + k_j^2}{(n_j + 1)^2 + k_j^2}, j = ord, ext, pow \tag{2}$$

where n and k are the real and the imaginary part of the index of refraction. The optical constants of calcite by Long et al. (1993) are used for the simulation of the different contributions of the reflectance. The synthetic spectra for each contribution are shown in Fig. 1, in the spectral range between 2.5 and 25 μm (400–4000 cm^{-1}). In the considered spectral range, calcite presents two strong bands at 7.0 μm, due to C–O stretching vibration, and at 11.4 μm, due to the bending vibration. A third, less intense, band is also generally present at 14 μm. However, due to its weakness compared to the others, it will
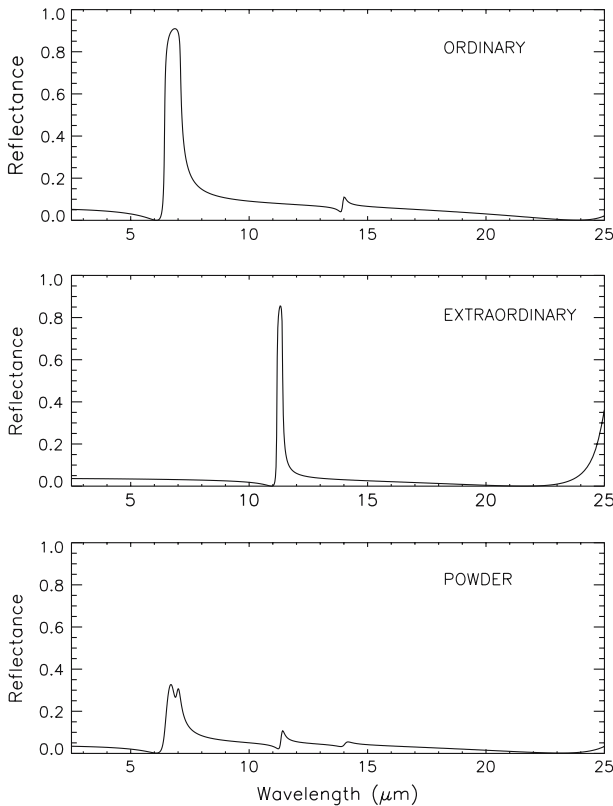
Fig. 1 Synthetic reflectance spectra of the ordinary, extraordinary mode and pressed powder computed by means of the Hapke formula and the calcite optical constants by Long et al. (1993)

not be considered in this work. As reported in Fig. 1, the first band is typical of the ordinary mode while the second band is due to the contribution of the extraordinary mode. The pressed powder spectrum presents, as expected, both the features modified in spectral contrast and, in the case of the 7.0 μm band, in shape with the presence of a double peak. Since the spectral contrast is strongly reduced by volume scattering when small particles contaminates the sample surface (Salisbury and Wald 1991), the 7.0 μm band appears the most appropriate in the role of diagnostic feature for detecting microfossil inclusions. It combines a reduction of the spectral contrast with a change in shape when powder is present inside the sample. In Fig. 2, the 7.0 μm calcite band is investigated in different sample conditions considering the typical measurement uncertainty of 3% for a reflectance spectrometer. Three combinations of ordinary and extraordinary modes are considered for the matrix (0.25–0.75, 0.50–0.50, 0.75–0.25) and four different amounts of powder inclusions of the whole sample (matrix plus inclusions) (0, 0.15, 0.30, 0.50). The resulting coefficients, used in Eq. 1, are reported in Table 1. Since the effects due to the powder presence are barely visible in correspondence to a 15% of powder content, this can be considered as the lower limit for the microfossil detectability in the considered measurement conditions.

2.2 Raman Spectroscopy

The static electric field E of an incident radiation of frequency v, induces, on a molecule with a proper vibration frequency v', a dipole momentum μ that, in a three-dimensional scalar form, can be written as

$$\mu_i = \alpha_{ij}E_j \tag{3}$$

where the indices run over the three dimensions. The square symmetric matrix of the α_{ij} components is known as the polarizability tensor. If Q_k is the normal coordinate of the fundamental mode v', such a mode is Raman-active if at least one of the six derivatives $\partial\alpha_{ij}/\partial Q_k$ is non-zero. The peak intensity of the derived spectral feature due to the single molecule (or unit cell) is proportional to $(\partial\alpha_{ij}/\partial Q_k)^2$ (Griffith 1974). Therefore, in the case of microfossil inclusions, each microdomain, within the microfossil inclusion, contributes in a different way to the spectral feature. If the number of microdomains seen by the field of view of the instrument is large, the peak intensity (I) of the considered Raman spectral feature is, in a first approximation,

$$I \propto \sum_n \left(\frac{\partial\alpha_{ij}}{\partial Q_k}\right)_n^2 \cos\theta_n \tag{4}$$

where θ_n is the angle between one selected cell axis and the direction of the incident light, and the sum takes into account the contribution of all the unit cells within each microdomain.

The typical field of view of a micro-Raman spectrometer produces a spot less than 5 μm in diameter, therefore much smaller than the dimension of a microfossil inclusion (see Fig. 3) but larger enough to contain many microdomains. Observing inside an inclusion, therefore, the unit calcite cells that contribute to the feature intensities are fully randomly oriented. On the contrary, observing a portion of the calcite matrix, the orientation of the unit cells can be considered inside a limited angular range around the plane of the
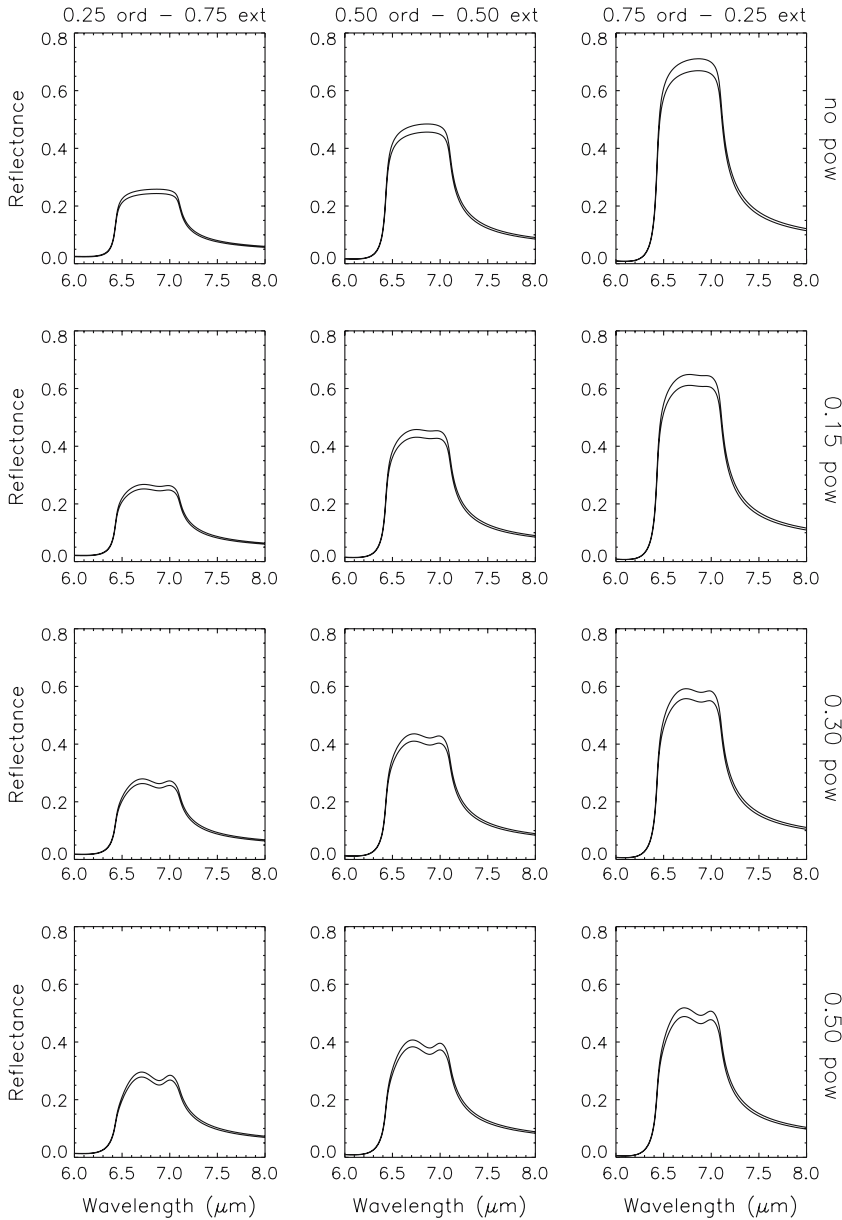
Fig. 2 Synthetic reflectance spectra for different sample conditions. On the top side it is reported the relative fraction of ordinary (ord) and extraordinary (ext) mode of the matrix and, on the right, the fraction of powder (pow) in the whole sample. For each spectrum the lines represent the typical measurement uncertainty (±3%)

sedimentary layer. The effect on the spectral feature of the microfossil inclusion is a decrease in the peak intensity with respect to the same feature seen in the matrix. A minor effect involves the width of the features, which increases keeping unchanged the area subtended by the band, producing a broadening of the Raman lines.

Table 1 Derived coefficients used to compute synthetic reflectance for different sample conditions

Matrix ord	Matrix ext	Inclusion	Area$_{ord}$	Area$_{ext}$	Area$_{pow}$
0.25	0.75	0	0.25	0.75	0
0.25	0.75	0.15	0.21	0.64	0.15
0.25	0.75	0.30	0.18	0.52	0.30
0.25	0.75	0.50	0.12	0.38	0.50
0.50	0.50	0	0.50	0.50	0
0.50	0.50	0.15	0.42	0.43	0.15
0.50	0.50	0.30	0.35	0.35	0.30
0.50	0.50	0.50	0.25	0.25	0.50
0.75	0.25	0	0.75	0.25	0
0.75	0.25	0.15	0.64	0.21	0.15
0.75	0.25	0.30	0.52	0.18	0.30
0.75	0.25	0.50	0.38	0.12	0.50
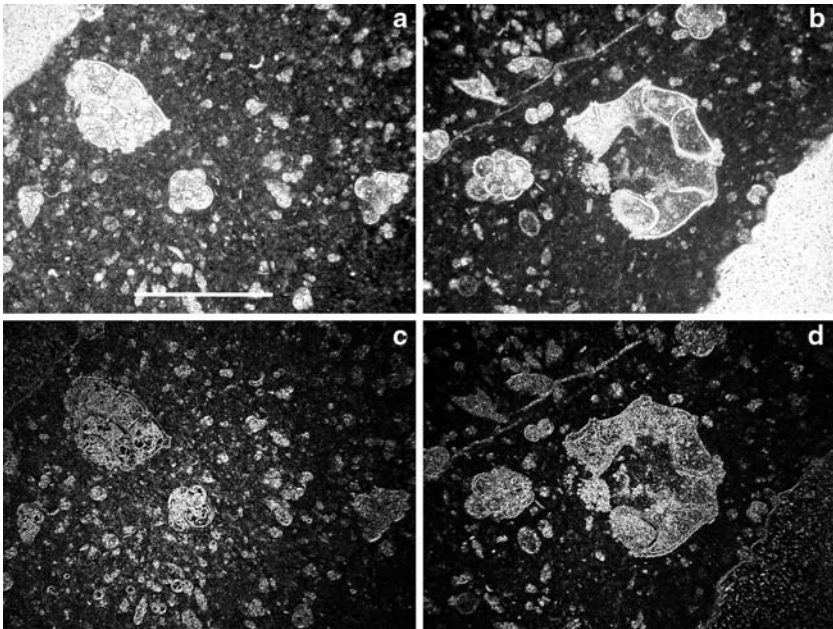
Fig. 3 Thin-sections micrographs in polarized light of the Upper Cretaceous sample (**a** and **b**) and the corresponding local contrast maps (**c** and **d**). The bar in plate a is 50 μm. The scale is the same for all the plates

To represent the Raman spectral features of calcite, we can suppose their behavior to be described by a Lorentzian function:

$$L(x) = \frac{1}{\pi} \frac{\frac{1}{2}\Gamma}{(x - x_0)^2 + \frac{1}{2}\Gamma} \qquad (5)$$

where x_0 is the position of the Lorentzian center in Raman shift, and Γ the Full Width at Half Maximum (FWHM) of the correspondent Raman feature.

In the usual Raman range of 200–4000 cm^{-1}, using a visible laser as a source of the exciting radiation (514.5 nm), the most prominent calcite feature, and therefore proper to be considered as diagnostic for microfossil detection, is the 1086 cm^{-1} band, due to the CO_3^{2-} symmetric stretching, which has a theoretical FWHM of about 2.2 cm^{-1} at a temperature of 300 K (Park 1966). In the ideal calcite matrix the angle in Eq. 4 can be considered as zero, providing the maximum peak intensity of the band normalized to 1. The computed synthetic 1086 cm^{-1} band is shown (dotted curve) in Fig. 4 compared with the case of total randomness in the angular distribution of the cells, which could represent the analogues to the internal structure of a microfossil inclusion.

In order to simulate the behaviour of the band intensity and width in the case of different orientations of the cells, the unitary peak intensity has been divided into a large number of contributions due to the single cells. The number of the contributing cells can be estimated, in a first approximation, by considering the shape of the exposed cell areas like a rectangle whose dimensions are those of the calcite crystallographic axes (*a* axis about 5 Å and *c* axis about 17 Å) (Sass et al. 1957). After dividing the sample area seen by the instrument field of view by the approximated area of the single cell corrected for the randomness orientation, the average contribution of the single cell was multiplied by cos θ, where θ is a random angle, computed by means of the Park and Miller (1988) algorithm which returns uniformly-distributed, floating-point numbers (Press et al. 1992). The values of θ have been picked up inside different ranges, representing different scenarios, going from the ideal calcite monocrystal (from 0° to 0°) to the completely random angular distribution of the cells (from –90° to +90°) with a 5° step. The computation has been repeated 10^3 times for each angular range and, by means of this procedure, we obtain a set of results spread within a statistical range. The extreme values of such a range are plotted in Fig. 4 with the addition of a ±3% taking into account the typical instrumental uncertainty. The result is that the peak intensity of an ideal Raman band of the matrix is reduced to about 65% in presence of a microfossil (Fig. 3). Such an effect is easily detectable by a Raman spectrometer.
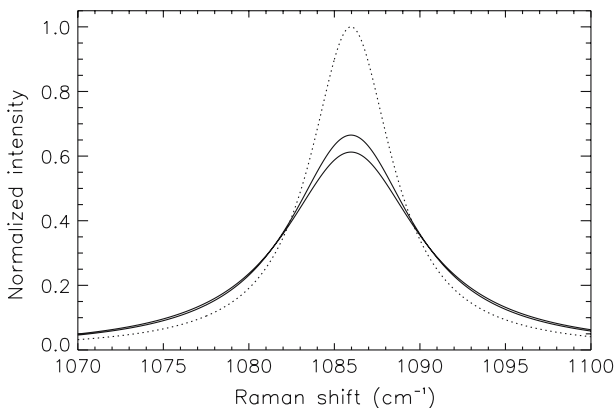
Fig. 4 Synthetic Raman 1086 cm^{-1} calcite band considering an ideal calcite matrix ($\theta = 0°$, dotted line) and for the completely random angular distribution of cells (–90° ≤ θ ≤ 90°, *solid lines*). The two solid lines represent the extreme values obtained with the computation described in the text

3 Laboratory Measurements

3.1 Sample

In order to check the possibility to detect the predicted effects, an appropriate sample has been selected. We decided to use a sample coming from a site with the following peculiar conditions: (1) a sedimentary calcitic deposit, and (2) an adequate density of microfossil inclusions. Such conditions are verified, for example, in the K–T sequence, a particular geological layer on Earth that separate the Cretaceous and the Tertiary layers, exposed near Gubbio (Italy), where the sequence corresponds to a calcitic sedimentary deposit. The K–T sequence is a geological sequence of layers dating back to about 65 million years ago. The Cretaceous (146–65 My ago) is known as the Age of Dinosaurs, since such giant reptiles were the dominant species. The Tertiary (65–2 My ago), for the same reason, is known as the Age of Mammals. The two geological eras are separated by what is known as the Cretaceous–Tertiary Mass Extinction event (K–T event). In fact about 70% of the living species, including the dinosaurs, disappeared within a very short period of time. One of the current explanations relates this mass extinction to the catastrophic impact of a large meteorite (Alvarez et al. 1980). This seems also suggested by the presence of an Iridium-rich layer, separating the two geological eras. In fact Iridium is fairly rare on Earth and such unusual abundance in a limited period of time has been explained by a possible extraterrestrial origin (Sigurdsson et al. 1991). Our sample comes from the Upper Cretaceous geological layer. It is extremely rich in extinct life forms and, therefore, in microfossil inclusions consisting of foraminifers. For a comprehensive characterization of the site, and therefore of the sample, from a biological and paleontological point of view, we refer the reader to Kuhnt (1990).

Thin-section micrographs of the sample using polarized light have been realized at the Dipartimento di Scienze della Terra–Università di Parma, Italy; two selected micrographs are reported in plate a and plate b of Fig. 3. Such images allow verifying the presence of microfossils into the sample compatible with those expected to occur in Gubbio (Kuhnt 1990) and in other K–T sites (Keller et al. 2004). The polarized light micrographs provide valuable information about the structure of crystallographic microdomains. In Fig. 3, both plate a and plate b show relatively homogeneous dark regions and structured bright inclusions. Dark colour indicates an ordered matrix where the lattice cells are disposed along a preferential direction, while bright structures are indicative of a high degree of disorder among the cells orientation, and indeed they identify the microfossil inclusions. Both images present a bright large corner, which is a not-lapped portion of the thin-section which preserves the natural fracture of the original rock. It appears as bright as the microfossil inclusions, but represents a region with a common orientation of the cells different with respect to the lapped matrix. In order to confirm this interpretation we have measured the contrast by means of the grey level co-occurrence matrix (GLCM), a method, originally described by Haralick et al. (1973), for the evaluation of the amount of local variations of the gray levels in an image. This method provides a map of local contrast where bright colour represents a high gray-level difference within each pixel pair. The contrast maps corresponding to plate a and plate b are reported in plate c and plate d of Fig. 3, respectively. In such maps microfossils keep their bright appearance while not-lapped regions become dark. This result demonstrates that microfossil inclusions are formed by random oriented lattice cells following the microorganism morphologies, while the not-lapped regions have homogeneous preferred orientations.

In order to perform the IR and Raman spectroscopic measurements, samples of the Upper Cretaceous layer have been roughly lapped on the side selected for the analysis, and a photographic sampling was performed in order to identify areas with large microfossils content. An area presenting unicellular microorganisms has been selected and used both for infrared reflectance and Raman analysis. In particular, in the analyzed area of our sample, some hundreds inclusions were observed, with a linear average dimension of about 250 μm.

3.2 Experimental Apparatus

The instrumentation used for laboratory measurements consists of an infrared spectrometer and a Raman system implemented ad hoc. The infrared spectrometer is a Perkin Elmer Spectrum 2000, a Fourier spectrometer performing infrared conical hemispherical reflectance spectroscopy, at 13°, in the range from 5 to 25 μm (400–2000 cm^{-1}). This configuration has a field of view of about 1 cm in diameter, which means that a very large number of microfossil inclusions are simultaneously observed.

Micro-Raman spectra have been collected, in the 250–1400 cm^{-1} Raman shift range, at the Laboratorio di Astrofisica Sperimentale (LASp-INAF) in Catania (Italy) using a system with the following specifications: an Ar^+ laser emitting radiation at 514.5 nm (laser power of about 5–10 mW on the sample, for 3–5 min.), a co-focal illuminator, an optical microscope with a 50× or a 10× objective producing a spot size on the sample respectively of 2–4 μm and 10–20 μm in diameter, a Triplemate SPEX spectrometer, and a CCD detector. A digital camera is also used for visual inspection of the samples by collecting images of the analyzed area through the microscope objective. The Raman spectrometer has a resolution of about 3 cm^{-1} in Raman shift and a positioning reproducibility of about 1 cm^{-1}.

3.3 Results

An infrared conical hemispherical reflectance spectrum of the selected portion of the K–T sample is reported in Fig. 5. The upper panel shows the spectrum collected in the whole spectral range, making it evident that the volume scattering has a major role. In such a case, in fact, the 11.4 μm band is basically turned into a trough and also the diagnostic 7.0 μm band is modified both in intensity and in shape. These volume scattering effects are due to the residual contamination of very small dust particles on the sample side used for the measurement (Salisbury and Wald 1991). Such an effect was expected because of the rough lapping procedure used to prepare the sample. In the bottom panel of Fig. 5, the diagnostic 7.0 μm band is reported, showing a shape compatible with the synthetic features reported in Fig. 2 and therefore suggesting the presence of microfossil inclusions. The comparison between the measured spectrum and the synthetic ones suggests a sample having a matrix composition of 50% ordinary contribution and 50% extraordinary contribution with a 30% of microfossil inclusions in the whole sample. However, the microfossils amount may be strongly overestimated due to the scattering effects.

The micro-Raman spectra have been measured by means of the 50× objective, selecting the area without inclusions, for matrix reference, and a central area of a selected microfossil where the conditions described by the model are supposed to be verified. The Raman spectrum of the matrix has been normalized to unity and the spectrum of the microfossil has been proportionally scaled. Both are reported in the upper panel of Fig. 6. The
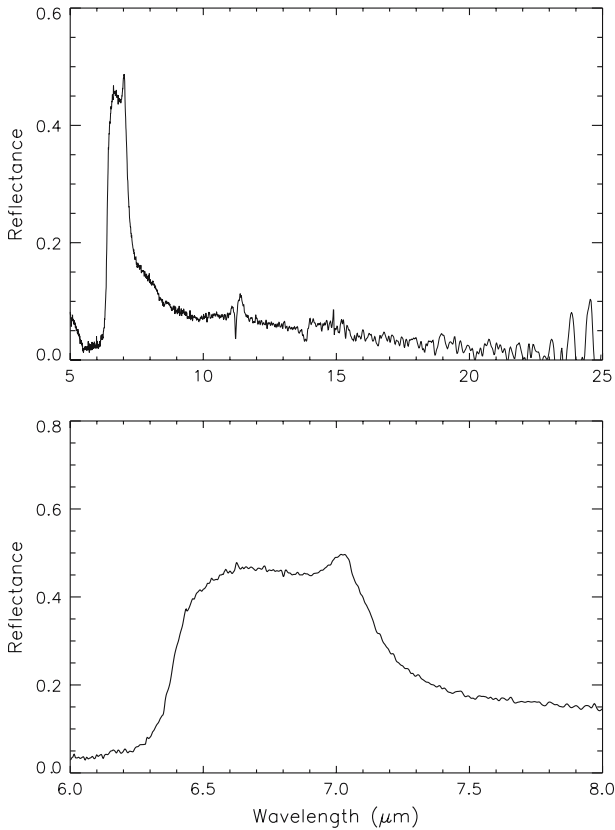
Fig. 5 Measured reflectance spectrum of the K–T sample (*upper panel*). Portion of the spectrum relative to the diagnostic feature of the microfossil presence (*bottom panel*)

1086 cm^{-1} band of the calcite, reported with greater detail in the bottom panel of Fig. 6, is observed to be reduced to 75% with respect to the same feature measured in sample area without the presence of microfossils. The broadening of the feature instead is not appreciable, as expected, due to the large instrument spectral resolution. It is necessary to observe that the estimated reduction amount of the 1086 cm^{-1} band, in the microfossil case, could be overestimated because the corresponding matrix feature is considered to be analogue to the ideal case. Moreover, we note that the other visible calcite feature, at 286 cm^{-1}, is also reduced in peak intensity, in the microfossil spectrum, with respect to the matrix. However, it is important to note that the peak intensities and the ratio among peak intensities of the Raman bands, can generally depend on many variables (Perez and Martinez-Frias 2003). In addition, we want to stress that, due to the low signal-to-noise ratio, all the above results have to be considered quite preliminary.

4 Discussions and Conclusions

The aim of the present work is to investigate the possibility of detecting the presence of microfossil inclusions in a mineral matrix by means of common spectroscopic techniques,
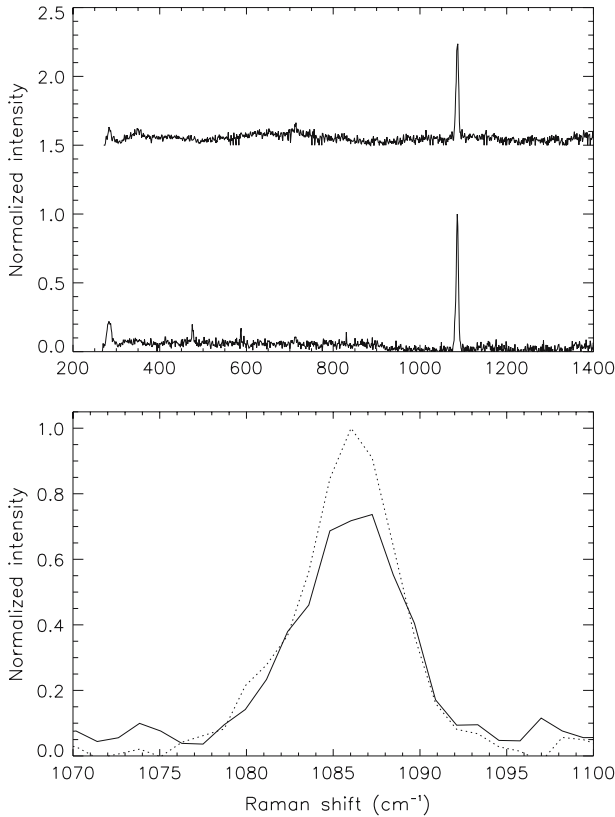
Fig. 6 In the upper panel, measured micro-Raman spectra of an area without microfossil inclusions (*bottom curve*) and a central area of a microfossil inclusion (*top curve*) are shown, with the latter vertically shifted by 1.5 in order to improve readability. In the bottom panel, a spectral enlargement of the same spectra (*not shifted*) is reported in order to compare the 1086 cm^{-1} feature outside (*dotted line*) and inside (*solid line*) the microfossil inclusion

such as infrared reflectance and Raman spectroscopy, that will be implemented on the next generation rovers for planetary exploration (Bellucci et al. 2003). The quantitative modeling of the fossilization process (in the examined case the mineral replacement of microorganisms in a sedimentary deposit of calcite) shows some effects, which can be detected with the above mentioned spectroscopic techniques. Such effects, although quite small, are detectable under favourable measurement conditions and, in connection with the visual context morphology analysis of the sample, can be useful to distinguish candidate areas with microfossils. They provide, therefore, additional information about the real presence of extinct life. However, both the investigated spectroscopic techniques provide no definite results because can be easily influenced by measurement conditions mimicking, or shadowing the microfossil presence. The volume scattering effect strongly modifies both the band strength and the shape of the infrared reflectance spectra. This effect is clearly visible in the spectrum reported in Fig. 5, and it is due to the presence of residual small particles produced by the lapping procedure on the sample side used for the measurements. On the other hand, the rough lapping does not influence the Raman spectra enough to shadow the degradation of the spectral features, but other types of inclusions,

such as impurities, can obviously produce the same spectral effects. A single-measurement approach is, therefore, not reliable to support the usual morphology investigations in search for the microfossil presence. Reflectance spectroscopy results can be improved by a better preparation of the sample, while Raman spectroscopy needs a complete set of measurements of the candidate area in order to exclude impurity effects, and to individuate residual organic matter that is expected in correspondence of microfossils (Schopf et al. 2002).

The foreseen effects, with both spectroscopic techniques, are based on the hypothesis of different lattice structures between the mineral matrix and the mineralized microfossil inclusions, and this hypothesis appears to be confirmed by polarized light microscopy, which is able to enhance sample areas with different lattice structures. In the near future, extensions of the model will be taken into account and measurement campaigns on different matrix materials will be performed in order to better investigate the potential of the techniques described in the present paper.

References

L.W. Alvarez, W. Alvarez, F. Asaro, H.V. Michel, Science **208**, 1095 (1980)

J.F. Banfield, J.W. Morreau, C.S. Chan, S.A. Welch, B. Little, Astrobiology **1**(4), 447 (2001)

G. Bellucci, F. Altieri, M. Blecka, R. Bonsignori, P. Coppo, S. Fonti, G. Marzo, S. Meli, J.J.L. Moreno, B. Moshkin, G.G. Ori, V. Orofino, R. Politi, G. Preti, A. Romoli, T. Roush, B. Saggin, M. Sgavetti, D. Stam, L. Zasova, in *Recent Developments in Astronomy and Astrophysics*, ed. by S.G. Pandalai (Research Signpost, Kerala, 2003), p. 839

J.P. Bibring, Y. Langevin, J.F. Mustard, F. Poulet, R. Arvidson, A. Gendrin, B. Gondet, N. Mangold, P. Pinet, F. Forget, Science **312**, 400 (2006)

F.P. Fanale, S.E. Postawko, J.B. Pollack, M.H. Carr, R.O. Pepin, in *Mars*, ed. by H.H. Kieffer. Mars: Epochal Climate Change and Volatile History, (The University of Ariziona Press, Tucson London, 1992), p. 1135

F. Forget, R.T. Pierrehumbert, Science **278**, 1273 (1997)

W.P. Griffith, in *The Infrared Spectra of Minerals*, ed. by V.C. Farmer. Raman Spectroscopy of Minerals, (Mineralogical Society, London, 1974), p. 119

B. Hapke, *Theory of Reflectance and Emittance Spectroscopy*, (Cambridge Univ. Press, New York, 1993), p. 48

R.M. Haralick, K. Shanmugam, I. Dinstein, IEEE Trans. on Systems, Man, and Cybernetics **SMC-3**(6), 610 (1973)

B.M. Hynek, R.J. Phillips, Geology **31**, 757 (2003)

A.D. Howard, J. M. Moore, R.P. Irwin, J. Geophys. Res. **110**, 12 (2005)

G. Keller, T. Adatte, W. Stinnesbeck, M. Rebolledo-Vieyra, J.U. Fucugauchi, U. Kramar, D. Stuben, PNAS **101**(11), 3753 (2004)

W. Kuhnt, Micropaleontology **34**(4), 297 (1990)

L.L. Long, M.R. Querry, R.J. Bell, R.W. Alexander, Infrared Phys. **34**, 191

M.C. Malin, M.H. Carr, (1999) Nature **397**, 589 (1993)

C.V. Mendelson, J.W. Schopf, in *The Proterozoic Biosphere: A Multidisciplinary Study*, ed. by J.W. Schopf C. Klein. Proterozoic and Selected Early Cambrian Microfossils and Microfossil-like Objects, (Cambridge Univ. Press, New York, 1992), p. 865

K. Park, Phys. Let. **22**, 39 (1966)

S.K. Park, K.W. Miller, Communications of the ACM **31**, 1192 (1988)

F.R. Perez, J. Martinez-Frias, J. Raman Spectrosc. **31**, 367 (2003)

J.B. Pollack, J.F. Kasting, S.M. Richarsson, K. Poliakoff, K. Icarus **71**, 203 (1987)

W.H. Press, B.P. Flannery, S.A. Teukolsky, W.T. Vetterling, *Numerical Recipes in C: The Art of Scientific Computing*, (Cambridge Univ. Press, New York, 1992), p. 275

J.W. Salisbury, A. Wald, Icarus **96**, 121 (1991)

R.L. Sass, R. Vidale, J. Donohue, Acta Cryst. **10**, 567 (1957)

J.W. Schopf, A.B. Kudryavtsev, D.G. Agresti, T.J. Wdowlak, A.D. Czaja, Nature **416**, 73 (2002)

J.W. Schopf M.R. Walter, in *Earth's Earliest Biosphere: Its Origin and Evolution*, ed. by J.W. Schopf. Archean Microfossils: New Evidence of Ancient Microbes, (Princeton Univ. Press, Princeton, 1983), p. 214

H. Sigurdsson, Ph. Bont, L. Turpin, M. Chaussidon, N. Metrich, M. Steinberg, Ph. Pradel, S. D'Hondt, Nature **353**, 839 (1991)

S.W. Squyres, J.F. Kasting, Science **265**, 744 (1994)

F. Westall, J. Geophys. Res. **104**(E7), 16,473 (1999)

Y.L. Yung, H. Nair, M.F. Gerstell, Icarus **130**, 222 (1997)